Inorg. Chem. **2009**, *48*, 4190−4200

Reduction Chemistry of Aryl- and Alkyl-Substituted Bis(imino)pyridine Iron Dihalide Compounds: Molecular and Electronic Structures of [(PDI)$_2$Fe] Derivatives

Bradley M. Wile,[†] Ryan J. Trovitch,[†] Suzanne C. Bart,[†] Aaron M. Tondreau,[†] Emil Lobkovsky,[†] Carsten Milsmann,[‡] Eckhard Bill,[‡] Karl Wieghardt,[‡] and Paul J. Chirik*[,†]

Department of Chemistry and Chemical Biology, Baker Laboratory, Cornell University, Ithaca, New York, 14853, and Max-Planck Institute of Bioinorganic Chemistry, Stiftstrasse 34-36, D-45470 Mülheim an der Ruhr, Germany

Received August 26, 2008

Sodium amalgam reduction of the aryl-substituted bis(imino)pyridine iron dibromide complex, (^{Et}PDI)FeBr$_2$ (^{Et}PDI = 2,6-(2,6-Et$_2$-C$_6$H$_3$N═CMe)$_2$C$_5$H$_3$N), under a dinitrogen atmosphere in pentane furnished the bis(chelate)iron compound, (^{Et}PDI)$_2$Fe. Characterization by X-ray crystallography established a distorted four-coordinate iron center with two κ^2-bis(imino)pyridine ligands. Reducing the steric demands of the imine substituent to either a less sterically encumbered aryl ring (e.g., C$_6$H$_4$-4-OMe) or an alkyl group (e.g., Cy, ^{i}Pr, *cis*-myrtanyl) also yielded bis(chelate) compounds from sodium amalgam reduction of the corresponding dihalide. Characterization of the compounds with smaller imine substituents by X-ray diffraction established six-coordinate, pseudo-octahedral compounds. In one case, a neutral bis(chelate)iron compound was prepared by reduction of the corresponding iron dication, [(PDI)$_2$Fe]$^{2+}$, providing chemical confirmation of electrochemically generated species that were previously reported as too reducing to isolate. Magnetic measurements, metrical parameters from X-ray structures, Mössbauer spectroscopy, and open-shell, broken symmetry DFT calculations were used to establish the electronic structure of both types (four- and six-coordinate) of neutral bis(chelate) compounds. The experimentally observed $S = 1$ compounds are best described as having high-spin ferrous ($S_{Fe} = 2$) centers antiferromagnetically coupled to two bis(imino)pyridine radical anions. Thus, the two-electron reduction of the diamagnetic, low-spin complex [(PDI)$_2$Fe]$^{2+}$ to [(PDI)$_2$Fe] is ligand-based with a concomitant spin change at iron.

Introduction

The discovery of ethylene and α-olefin polymerization by methylaluminoxane-activated aryl-substituted bis(imino)pyridine iron dihalide compounds has spawned intense interest in this class of compounds for both polymer and small molecule catalysis.[1] Modification of the imine aryl substituents is known to influence the outcome of the polymerization. For example, 2,6-disubstituted precatalysts yield regioregular, moderately isotactic polypropylene,[2] whereas those bearing a single methyl or 2,6-difluoro substituents are selective for α-olefin production.[3−6] In small-molecule catalysis, the sterically protected bis(imino)pyridine iron dinitrogen complex, (^{iPr}PDI)Fe(N$_2$)$_2$[7] (^{iPr}PDI = 2,6-(2,6-^{i}Pr$_2$−C$_6$H$_3$N═CMe)$_2$C$_5$H$_3$N), is effective for the hydrogena-

* Author to whom correspondence should be addressed. E-mail: pc92@cornell.edu.
† Cornell University.
‡ Max-Planck Institute of Bioinorganic Chemistry.

(1) (a) Bianchini, C.; Giambastiani, G.; Rios, I. G.; Mantovani, G.; Meli, A.; Segarra, A. M. *Coord. Chem. Rev.* **2006**, *250*, 1391. (b) Small, B. L.; Brookhart, M.; Bennett, A. M. A. *J. Am. Chem. Soc.* **1998**, *120*, 4049. (c) Britovsek, G. J. P.; Gibson, V. C.; Kimberley, B. S.; Maddox, P. J.; McTavish, S. J.; Solan, G. A.; White, A. J. P.; Williams, D. J. *Chem. Commun.* **1998**, 849.
(2) Small, B. L.; Brookhart, M. *Macromolecules* **1999**, *32*, 2120.
(3) Ionkin, A. S.; Marshall, W. J.; Adelman, D. J.; Fones, B. B.; Fish, B. M.; Schiffhauer, M. F. *Organometallics* **2008**, *27*, 1147.
(4) Schmid, M.; Eberhardt, R.; Klinga, M.; Leskela, M.; Rieger, B. *Organometallics* **2001**, *20*, 2321.
(5) Ionkin, A. S.; Marshall, W. J. *Organometallics* **2004**, *23*, 3276.
(6) Alt, H. G.; Licht, E. H.; Licht, A. I.; Schneider, K. J. *Coord. Chem. Rev.* **2006**, *250*, 2.
(7) Bart, S. C.; Lobkovsky, E.; Chirik, P. J. *J. Am. Chem. Soc.* **2004**, *126*, 13794.
(8) Bouwkamp, M. W.; Bowman, A. C.; Lobkovsky, E.; Chirik, P. J. *J. Am. Chem. Soc.* **2006**, *128*, 13340.
(9) Trovitch, R. J.; Lobkovsky, E.; Bill, E; Chirik, P. J. *Organometallics* **2008**, *27*, 1470.

10.1021/ic801623m CCC: $40.75
Published on Web 11/26/2008

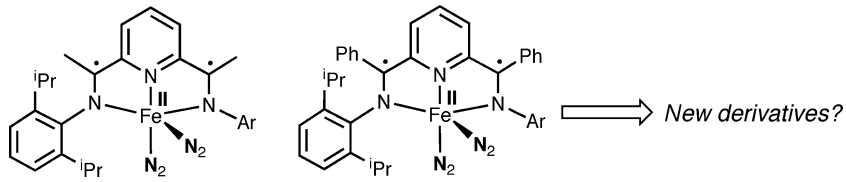

Figure 1. Catalytically active bis(imino)pyridine iron dinitrogen complexes.

tion, hydrosilylation,[7] and $[2\pi + 2\pi]$ cycloisomerization of olefins.[8] For many examples, efficient turnover and broad functional group tolerance were observed.[9]

In addition to its catalytic performance, (^{iPr}PDI)Fe(N_2)$_2$ also exhibits an interesting electronic structure. Spectroscopic, structural, and computational studies established an intermediate spin ferrous center complexed by a doubly reduced bis(imino)pyridine chelate dianion.[10] In addition to their well-established redox-activity,[11,12] bis(imino)pyridines are attractive ligands for iron chemistry due to their low cost, air stability, and straightforward synthesis.[13] Typically, these compounds are prepared by the condensation of 2 equiv of the appropriate amine with 2,6-diacetylpyridine. This method has been exploited for the preparation of libraries of ligands derived from anilines and aliphatic amines, as well as other nonhydrocarbyl substituents.[1a]

Motivated by the rich chemistry of (^{iPr}PDI)Fe(N_2)$_2$ in catalytic processes and group transfer reactions,[14,15] we sought to prepare libraries of new bis(imino)pyridine iron bis(dinitrogen) complexes to expand the scope, activity, and selectivity of iron-catalyzed reactions (Figure 1). The only other bis(imino)pyridine iron bis(dinitrogen) compound reported to date is the case where the imine methyl groups have been replaced with phenyl substituents.[16] This compound exhibits higher activity than (^{iPr}PDI)Fe(N_2)$_2$ for the catalytic hydrogenation and hydrosilylation of simple, unactivated alkenes, although competing η^6-arene coordination was identified as a significant catalyst deactivation pathway. Similar η^6-aryl coordination was observed for (^{iPr}PDI)Fe(N_2)$_2$, but much higher temperatures were required.[17]

Here, we describe our efforts to synthesize analogs of (^{iPr}PDI)Fe(N_2)$_2$ with both aryl- and alkyl-substituted bis(imino)pyridines. Reduction of the corresponding dibromide complexes furnished a family of paramagnetic, bis(chelate)iron complexes. The electronic structures of these compounds were elucidated by a combination of X-ray diffraction, SQUID magnetometry, Mössbauer spectroscopy, NMR spectroscopy, and DFT calculations.

Results and Discussion

Reduction of Aryl- and Alkyl-Substituted Bis(imino)pyridine Iron Dihalide Complexes. Because of the structural similarity of the 2,6-diethyl-substituted bis(imino)pyridine iron complex to the previously reported bis(dinitrogen) compounds, the reduction of the corresponding ferrous dibromide, (^{Et}PDI)FeBr_2, was initially examined. Mimicking the conditions used to prepare (^{iPr}PDI)Fe(N_2)$_2$,[7] a pentane slurry of (^{Et}PDI)FeBr_2 was stirred in the presence of excess 0.5% sodium amalgam under a dinitrogen atmosphere. Filtration and recrystallization from pentane at −35 °C furnished a brown solid that was not the desired bis(imino)pyridine iron dinitrogen compound but rather the paramagnetic iron bis(chelate) derivative, (^{Et}PDI)$_2$Fe (eq 1).

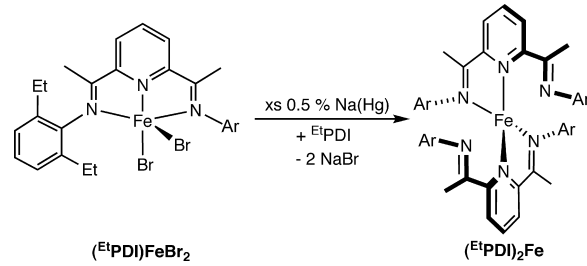

(1)

After the reduction product of (^{Et}PDI)FeBr_2 was identified as the bis(chelate)iron compound, (^{Et}PDI)$_2$Fe, the synthetic procedure was modified to include an additional equivalent of free bis(imino)pyridine ligand. This alteration improved the isolated yield to 55% following recrystallization. The benzene-d_6 ^{1}H NMR spectrum of paramagnetic (^{Et}PDI)$_2$Fe exhibits four diagnostic, broad peaks that are not readily assigned but which are useful as a means of confirming the presence of the compound in solution.

The isolation of (^{Et}PDI)$_2$Fe from sodium amalgam reduction of the corresponding bis(imino)pyridine iron dibromide is reminiscent of the electrochemically generated bis(chelate)iron complexes previously reported by Toma et al.[18,19] and subsequently by Wieghardt and co-workers.[11] In these studies, the [(PDI)$_2$Fe] complexes were the least well-characterized, owing to their "extraordinarily strong reducing power".[11] Specifically, solutions of $[(PDI)_2Fe]^{2+}$ were electrochemically reduced and the resulting monocationic and neutral species identified by electronic absorption spectroscopy. These studies are seminal examples of the redox activity of bis(imino)pyridine ligands in reduced transition metal chemistry.[10,12]

Inspired by these observations, the preparation and subsequent chemical reduction of $[(^{Et}PDI)_2Fe]^{2+}$ was targeted.

(10) Bart, S. C.; Chlopek, K.; Bill, E.; Bouwkamp, M. W.; Lobkovsky, E.; Neese, F.; Wieghardt, K.; Chirik, P. J. *J. Am. Chem. Soc.* **2006**, *128*, 13901.
(11) de Bruin, B.; Bill, E.; Bothe, E.; Weyhermüller, T.; Wieghardt, K. *Inorg. Chem.* **2000**, *39*, 2936.
(12) Knijnenburg, Q.; Gambarotta, S.; Budzelaar, P. H. M. *Dalton Trans.* **2006**, 5442.
(13) Gibson, V. C.; Redshaw, C.; Solan, G. A. *Chem. Rev.* **2007**, *107*, 1745.
(14) Bart, S. C.; Lobkovsky, E.; Bill, E.; Chirik, P. J. *J. Am. Chem. Soc.* **2006**, *128*, 5302.
(15) Bart, S. C.; Bowman, A. C.; Lobkovsky, E.; Chirik, P. J. *J. Am. Chem. Soc.* **2007**, *129*, 7212.
(16) Archer, A. M.; Bouwkamp, M. W.; Cortez, M.-P.; Lobkovsky, E.; Chirik, P. J. *Organometallics* **2006**, *25*, 4269.
(17) Trovitch, R. J.; Lobkovsky, E.; Chirik, P. J. *Organometallics* **2008**, ASAP (DOI: 10.1021/om8005596).
(18) Kuwabara, I. H.; Comninos, F. C. M.; Pardini, V. L.; Viertler, H.; Toma, H. E. *Electrochim. Acta* **1994**, *39*, 2401.
(19) Toma, H. E.; Chavez-Gil, T. E. *Inorg. Chim. Acta* **1997**, *257*, 197.

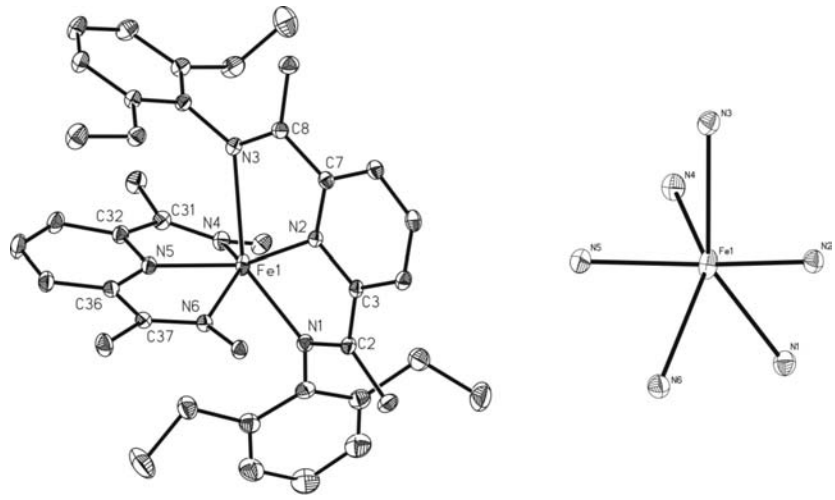

Figure 2. Molecular structure of (^{Et}PDI)$_2$Fe at 30% probability ellipsoids. Hydrogen atoms and aryl groups on one bis(imino)pyridine ligand omitted for clarity. A view of the core of the molecule is presented on the right.

Treatment of (^{Et}PDI)FeBr$_2$ with NH_4PF_6 in methanol[11] was unsuccessful, yielding a mixture of unidentified products. Attempts to prepare [(^{iPr}PDI)$_2$Fe](PF$_6$)$_2$ using a similar method were also unsuccessful, highlighting the ability of sterically demanding aryl substituents to prevent the formation of dicationic bis(chelate)iron compounds. Because such compounds could not be isolated, attention was devoted to bis(imino)pyridine iron complexes with smaller aryl substituents.

Previously, Wieghardt and co-workers reported the synthesis and electrochemical reduction of [($^{4\text{-OMe}}$PDI)$_2$Fe](PF$_6$)$_2$.[11] In the course of these studies, ($^{4\text{-OMe}}$PDI)$_2$Fe was spectroscopically observed but not isolated or crystallographically characterized. Sodium amalgam reduction of a toluene slurry of either [($^{4\text{-OMe}}$PDI)$_2$Fe](PF$_6$)$_2$ or ($^{4\text{-OMe}}$PDI)FeBr$_2$[20] furnished an olive green crystalline solid identified as the desired neutral bis(chelate) compound, ($^{4\text{-OMe}}$PDI)$_2$Fe (eq 2).

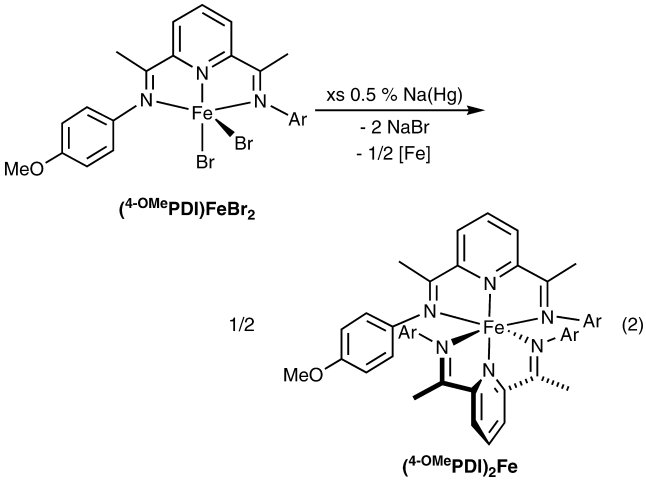

($^{4\text{-OMe}}$PDI)FeBr$_2$

($^{4\text{-OMe}}$PDI)$_2$Fe

To confirm that the isolated material, ($^{4\text{-OMe}}$PDI)$_2$Fe, was identical to the electrochemically generated species, the electronic absorption spectrum of the green product was recorded in a toluene solution at 23 °C. Peaks identical to those reported previously were observed,[11] confirming that the two compounds are indeed the same. Representative spectra for ($^{4\text{-OMe}}$PDI)$_2$Fe and (^{iPr}APDI)$_2$Fe along with peak maxima and extinction coefficients are reported in the Supporting Information. Importantly, chemical reduction of [(PDI)$_2$Fe]$^{2+}$ compounds can be used to prepare the corresponding neutral bis(chelate)iron derivatives, [(PDI)$_2$Fe].

Performing the reduction in the presence of excess free ligand did not increase the yield of ($^{4\text{-OMe}}$PDI)$_2$Fe, resulting principally in the recovery of the added bis(imino)pyridine. The ^{1}H NMR spectrum to (^{Et}PDI)$_2$Fe, the ^{1}H NMR spectrum of ($^{4\text{-OMe}}$PDI)$_2$Fe in benzene-d_6 at 23 °C exhibits seven paramagnetically shifted and broadened peaks.

Reduction of alkyl-substituted bis(imino)pyridine iron dibromide compounds was also explored. Interest in these compounds is derived from their ease of synthesis using a broad spectrum of commercially available (including chiral) amines as well as the superior performance of (^{Cy}APDI)Fe(CH$_2$SiMe$_3$)$_2$ (^{Cy}APDI = 2,6-(C$_6$H$_{11}$N═CMe)$_2$C$_5$H$_3$N) in catalytic aldehyde and ketone hydrosilylation reactions.[21]

Sodium amalgam reduction of toluene or pentane slurries of (^{Cy}APDI)FeBr$_2$, (^{iPr}APDI)FeBr$_2$, and (^{Myr}APDI)FeBr$_2$ followed by filtration and recrystallization furnished dark green solids identified as the corresponding bis(chelate)iron compounds (eq 3). The benzene-d_6 ^{1}H NMR spectra of paramagnetic (^{Cy}APDI)$_2$Fe, (^{iPr}APDI)$_2$Fe, and (^{Myr}APDI)$_2$Fe are similar to those observed for ($^{4\text{-OMe}}$PDI)$_2$Fe and exhibit more features than (^{Et}PDI)$_2$Fe.

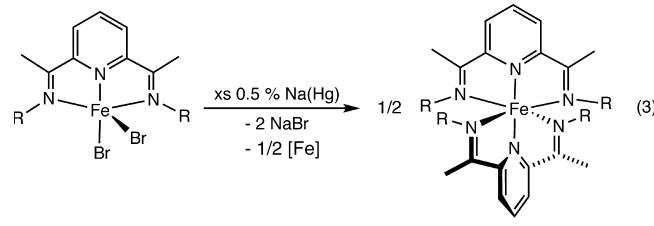

(^{Cy}APDI)$_2$Fe: R = Cy
(^{iPr}APDI)$_2$Fe: R = ^{i}Pr
(^{Myr}APDI)$_2$Fe: R = *cis*-myrtanyl

X-Ray Crystallographic Studies. Several of the neutral bis(chelate)iron compounds prepared in this work were

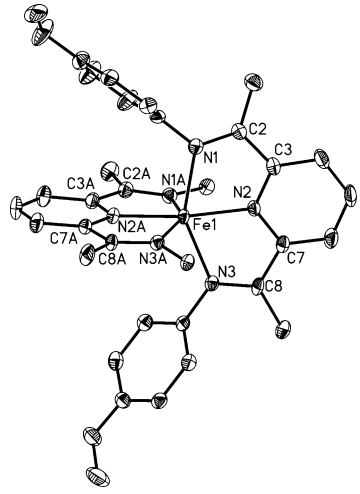

Figure 3. Molecular structure of ($^{4\text{-OMe}}$PDI)$_2$Fe at 30% probability ellipsoids. Hydrogen atoms and aryl rings on one bis(imino)pyridine chelate removed for clarity.

characterized by single-crystal X-ray diffraction. High-quality metrical parameters allow an accurate determination of ligand distortions that are diagnostic of redox activity[10−12] and provide interesting comparisons to structurally characterized [($^{4\text{-OMe}}$PDI)$_2$Fe](PF$_6$)$_2$.[11] The solid-state structure of ($^{\text{Et}}$PDI)$_2$Fe is presented in Figure 2, and selected bond distances and angles are reported in Table 1. Two independent iron molecules were located in the asymmetric unit as well as pentane and diethyl ether molecules from recrystallization. Because the two molecules differ only slightly, only one is presented and discussed in detail.

One salient feature of the solid-state structure of ($^{\text{Et}}$PDI)$_2$Fe is the deviation from a hexacoordinate, idealized octahedral geometry to a distorted tetrahedral environment with two κ^2-bis(imino)pyridine ligands. Each ligand has an imine "arm" at a long distance ($d_{\text{Fe-N}}$ = 2.6096(16) and 2.5579(16) Å), well outside the sum of the covalent radii for iron (1.25 Å) and nitrogen (0.75 Å). The κ^2- versus κ^3-bis(imino)pyridine is likely steric in origin; the relatively large 2,6-diethyl aryl substituents prevent formation of a bona fide six-coordinate compound. The nonbonding imine on each chelate allows for an internal comparison of ligand distortions diagnostic of redox activity. The coordinated $C_{\text{imine}}-N_{\text{imine}}$ distances of 1.332(2) and 1.334(3) Å are elongated from the value of 1.291(2) Å for both free imines. Likewise, the $C_{\text{imine}}-C_{\text{pyridine}}$ distances of 1.435(3) Å of the coordinated portion of the chelate are contracted compared to the 1.478(3) and 1.481(3) Å bond lengths found in the free "arms". These distortions are diagnostic of single-electron reduction on each chelate,[10,12] analogous to other reduced iron compounds with bidentate nitrogen donor ligands.[22]

The solid-state structure of ($^{4\text{-OMe}}$PDI)$_2$Fe, presented in Figure 3, established an octahedral geometry for the complex with less sterically protected imine aryl substituents. The overall molecular symmetry is idealized D_{2d} with an S_4 axis that relates C(1) and C(1A), N(1) and N(1A), and so forth. Selected bond distances and angles for ($^{4\text{-OMe}}$PDI)$_2$Fe are reported in Table 2. Also contained in Table 2 are the previously reported[11] bond distances for [($^{4\text{-OMe}}$PDI)$_2$Fe]$^{2+}$, where the chelate is undoubtedly in its neutral form and the ferrous ion is low-spin. The metrical parameters of both bis(imino)pyridines in the neutral compound are consistent with one-electron reduction, as previously proposed by Wieghardt and co-workers for the electrochemically generated species.[11] Most pronounced is the contraction of the $C_{\text{imine}}-C_{\text{pyridine}}$ bond lengths. In the reduced compounds, these values are 1.444(3) and 1.432(3) Å, similar to those reported ($C_{\text{imine}}-C_{\text{pyridine}}$ = 1.442(2), 1.441(2), 1.440(2), and 1.443(2) Å) for the related manganese cation, [($^{4\text{-OMe}}$PDI)$_2$Mn$^{\text{III}}$]$^+$, where one-electron reduced chelates are proposed.[11] One other notable feature of the metrical parameters are the changes in iron−nitrogen bond lengths upon the reduction of [($^{4\text{-OMe}}$PDI)$_2$Fe]$^{2+}$ to ($^{4\text{-OMe}}$PDI)$_2$Fe. Statistically significant lengthening of each of these bonds is observed with the addition of two electrons, suggesting a spin change from low to high spin at iron. More evidence for this effect will be presented in a later section of the article.

Two other bis(chelate)iron compounds, ($^{\text{Cy}}$APDI)$_2$Fe and ($^{\text{iPr}}$APDI)$_2$Fe, were also characterized by X-ray diffraction. Representations of the molecular structures are presented in Figure 4; selected bond distances and angles are reported in

Table 1. Selected Bond Distances (Å) and Angles (deg) for ($^{\text{Et}}$PDI)$_2$Fe

Fe(1)−N(1)	2.1246(16)
Fe(1)−N(2)	1.9853(15)
Fe(1)−N(3)	2.5579(16)
Fe(1)−N(4)	2.1098(16)
Fe(1)−N(5)	1.9864(15)
Fe(1)−N(6)	2.6096(16)
N(1)−C(2)	1.332(2)
N(2)−C(3)	1.390(2)
N(2)−C(7)	1.367(2)
N(3)−C(8)	1.291(2)
C(2)−C(3)	1.435(3)
C(7)−C(8)	1.478(3)
N(4)−C(31)	1.334(3)
N(5)−C(32)	1.387(2)
N(5)−C(36)	1.369(2)
N(6)−C(37)	1.291(2)
C(31)−C(32)	1.435(3)
C(36)−C(37)	1.481(3)
N(1)−Fe(1)−N(2)	78.99(6)
N(4)−Fe(1)−N(5)	79.44(6)
N(1)−Fe(1)−N(4)	101.15(6)
N(2)−Fe(1)−N(5)	138.95(6)

Table 2. Selected Bond Distances (Å) and Angles (deg) for ($^{4\text{-OMe}}$PDI)$_2$Fe

	($^{4\text{-OMe}}$PDI)$_2$Fe	[($^{4\text{-OMe}}$PDI)$_2$Fe]$^{2+}$ (ref 10)
Fe(1)−N(1)	2.1481(19)	1.974(2), 1.999(2)
Fe(1)−N(2)	2.0166(18)	1.8707(14), 1.8655(14)
Fe(1)−N(3)	2.1278(19)	1.9817(14), 1.9922(14)
N(1)−C(2)	1.306(3)	1.306(2), 1.309(2)
N(2)−C(3)	1.357(3)	1.356(2), 1.351(2)
N(2)−C(7)	1.370(3)	1.355(2), 1.351(2)
N(3)−C(8)	1.313(3)	1.311(2), 1.311(2)
C(2)−C(3)	1.444(3)	1.466(2), 1.466(2)
C(7)−C(8)	1.432(3)	1.466(2), 1.470(2)
N(1)−Fe(1)−N(3)	148.17(7)	159.09(6), 159.69(6)
N(1)−Fe(1)−N(1A)	100.44(7)	99.70(6)
N(2)−Fe(1)−N(2A)	171.76(11)	178.80(6)

(20) Bluhm, M. E.; Folli, C.; Döring, M. *J. Mol. Catal. A* **2004**, *212*, 13.
(21) Tondreau, A. M.; Lobkovsky, E.; Chirik, P. J. *Org. Lett.* **2008**, *10*, 2789.
(22) Muresan, N.; Lu, C. C.; Ghosh, M.; Peters, J. C.; Abe, M.; Henling, L. M.; Weyhermüller, T.; Bill, E.; Wieghardt, K. *Inorg. Chem.* **2008**, *47*, 4579.

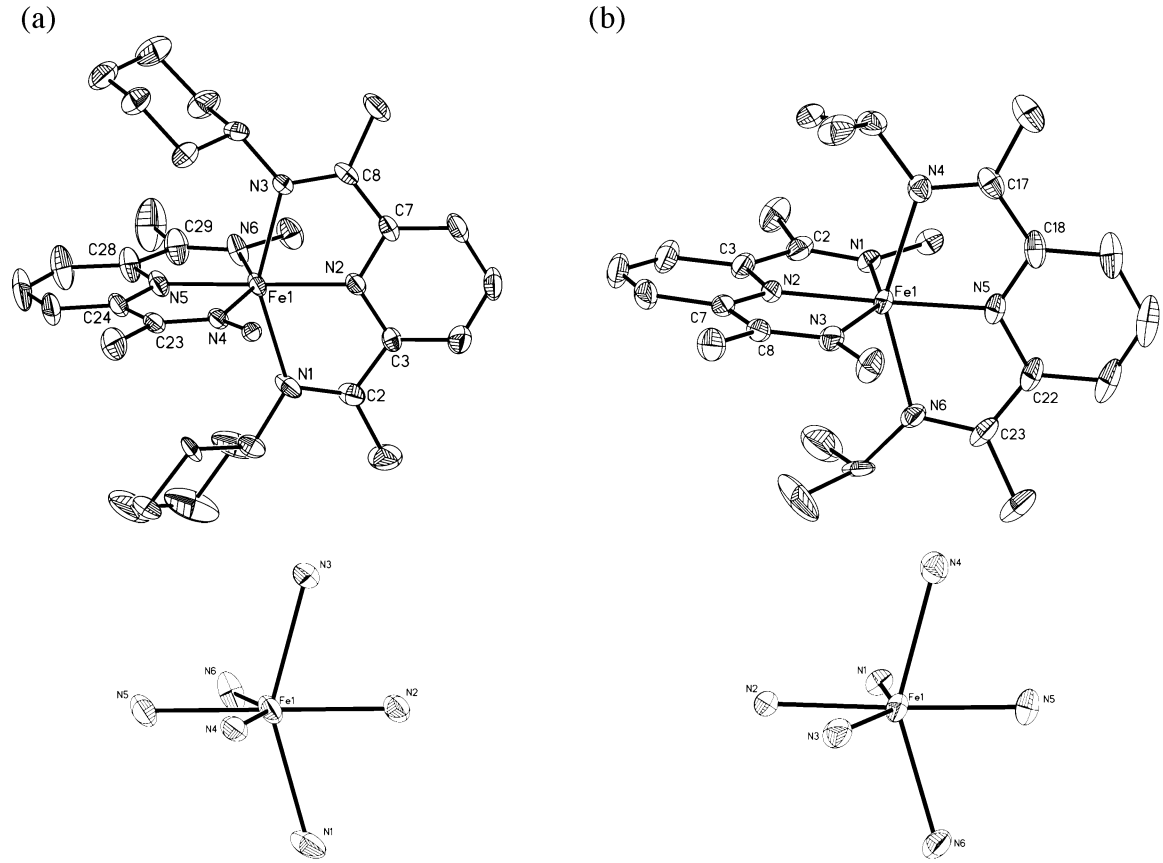

Figure 4. Molecular structures of (a) $(^{Cy}APDI)_2Fe$ and (b) $(^{iPr}APDI)_2Fe$ at 30% probability ellipsoids. Hydrogen atoms and selected imine substituents removed for clarity. View of the cores of the molecules are presented below each structure.

Table 3. Selected Bond Distances (Å) and Angles (deg) for $(^{Cy}APDI)_2Fe$ and $(^{iPr}APDI)_2Fe$

	$(^{Cy}APDI)_2Fe$	$(^{iPr}APDI)_2Fe$
Fe(1)−N(1)	2.243(2)	2.252(2)
Fe(1)−N(2)	2.005(2)	2.0180(17)
Fe(1)−N(3)	2.221(2)	2.2506(19)
Fe(1)−N(4)	2.209(2)	2.259(2)
Fe(1)−N(5)	2.005(2)	2.0236(18)
Fe(1)−N(6)	2.277(3)	2.1846(18)
N(1)−C(2)	1.293(4)	1.316(3)
N(2)−C(3)	1.384(4)	1.399(3)
N(2)−C(7)	1.375(3)	1.362(3)
N(3)−C(8)	1.310(3)	1.299(3)
C(2)−C(3)	1.437(4)	1.431(3)
C(7)−C(8)	1.442(4)	1.457(4)
N(4)−C(23)[a]	1.303(3)	1.312(3)
N(5)−C(24)	1.380(4)	1.387(3)
N(5)−C(28)	1.386(4)	1.358(3)
N(6)−C(29)	1.282(4)	1.304(3)
C(23)−C(24)	1.443(4)	1.426(3)
C(28)−C(29)	1.445(5)	1.450(4)
N(1)−Fe(1)−N(3)	149.64(8)	149.37(7)
N(4)−Fe(1)−N(6)	149.25(9)	149.06(7)
N(1)−Fe(1)−N(4)	93.01(8)	94.99(7)
N(2)−Fe(1)−N(5)	176.46(10)	176.90(8)

[a] For purposes of the table, the numbering scheme for $(^{Cy}APDI)_2Fe$ is used for $(^{iPr}APDI)_2Fe$.

Table 3. Both molecules have hexacoordinate geometries similar to that observed with $(^{4\text{-}OMe}PDI)_2Fe$. For $(^{Cy}APDI)_2Fe$, the cyclohexyl substituents on the imine ligands are disordered. The disorder was successfully modeled, and reliable metrical parameters for the core of the molecule were obtained. However, the $C_{imine}-N_{imine}$ expansions and the $C_{imine}-C_{pyridine}$ contractions are consistent with one-electron reduction (Table 3).[10−12]

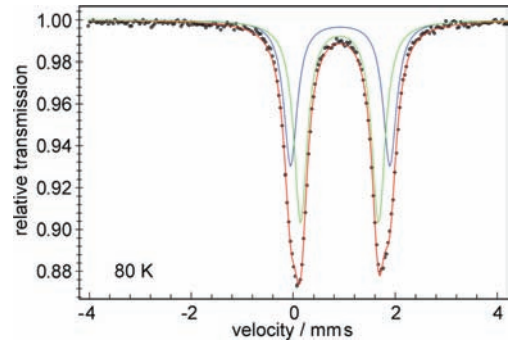

Figure 5. Zero-field Mössbauer spectrum of $(^{Et}PDI)_2Fe$ at 80 K.

Magnetochemistry and Mössbauer Spectroscopy. The electronic structures of the neutral bis(imino)pyridine bis(chelate) compounds were further investigated with magnetochemistry and Mössbauer spectroscopy. Because of the gross structural difference between $(^{Et}PDI)_2Fe$ and the other bis(chelate)iron compounds prepared in this work, $(^{Et}PDI)_2Fe$ will be treated separately. The zero-field Mössbauer spectrum of $(^{Et}PDI)_2Fe$ was recorded at 80 K and is presented in Figure 5. Two subspectra with similar isomer shifts, $\delta = 0.91$ and 0.92 mm s^{-1}, and quadrupole splittings, $\Delta E_Q = 1.53$ and 1.95 mm s^{-1}, were obtained reproducibly from independently prepared, analytically pure samples and are likely a result of the two independent forms of the molecule found in the

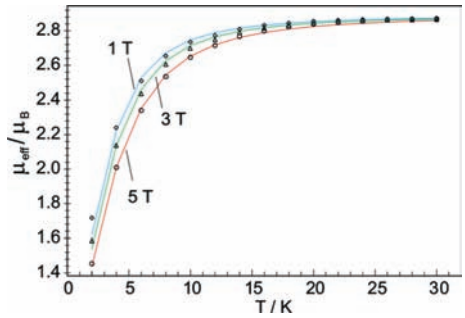

Figure 6. Variable-temperature SQUID magnetic data for (^{Et}PDI)$_2$Fe measured at 1, 3, and 5 T. The solid lines are simulations for $S_t = 1$ with the parameters given in the text.

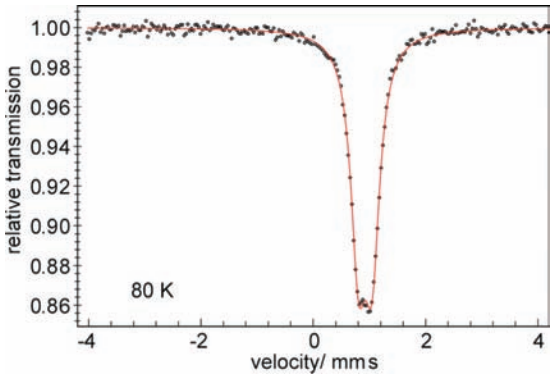

Figure 7. Zero-field Mössbauer spectrum of (^{iPr}APDI)$_2$Fe at 80 K.

crystal lattice. The Mössbauer parameters clearly characterize (^{Et}PDI)$_2$Fe as a high-spin iron(II) complex.

Temperature-dependent solid-state magnetic susceptibility measurements on (^{Et}PDI)$_2$Fe (Figure 6) established a plateau at 2.83 μ_B. This value is similar to the benzene-d_6 solution value of 2.7 μ_B measured at 23 °C. It reveals a total spin triplet for the ground state of the compound, which apparently owes its origin to the antiferromagnetic exchange coupling of iron(II), $S_{Fe} = 2$, and two ligand radicals ($S_{rad} = 1/2$). The ground state is well separated from excited states by 1000 cm^{-1} or more, since no thermal population of excited states with higher spin is observed up to $T = 300$ K. This yields a lower limit for the exchange coupling constant of about -240 cm^{-1} (radical−radical coupling neglected). The temperature dependence of the solid-state magnetic moment exhibits a downward slope in the linear portion of the curve between approximately 10 and 300 K. A spin-Hamiltonian simulation with $S_t = 1$ yielded the following parameters: $g_t = 2.04$ and $|D_t| = 8.8$ cm^{-1} (rhombicity, E/D was neglected). From these numbers, the local values for iron can be obtained from the relation $D_{Fe} = 10/21D_t$, $g_{Fe} = 2/3g_t + 1/3g_{rad}$, derived from spin projection. The result, $D_{Fe} = 4.2$ cm^{-1} and $g_{Fe} = 2.03$ (assuming $g_{rad} = 2$), is consistent with a high-spin ferrous ion in a tetrahedral ligand field.

The zero-field Mössbauer spectrum of a six-coordinate bis(chelate) complex was also determined. The data recorded at 80 K for (^{iPr}APDI)$_2$Fe are presented in Figure 7 and produced an isomer shift (δ) of 0.93 mm s^{-1} and quadrupole splitting (ΔE_Q) of 0.24 mm s^{-1}. Whereas the isomer shift clearly reveals high-spin iron(II), the small quadrupole splitting is relatively rare for an iron(II) compound and demonstrates a minimal electric field gradient at the ^{57}Fe nucleus. A smaller ΔE_Q value of 0.073 mm s^{-1} was measured for $CsFe(H_2O)_6PO_4$ and was interpreted as having deviations from cubic symmetry that are minimal.[23] The isomer shifts for (^{Et}PDI)$_2$Fe and (^{iPr}APDI)$_2$Fe are significantly higher than the values of 0.235 and 0.238 mm s^{-1} reported for the low-spin, diamagnetic [($^{4\text{-OMe}}$PDI)$_2$Fe](PF$_6$)$_2$[11] and [(terpy)$_2$Fe](ClO$_4$)$_2$ (terpy = terpyridine).[24]

Table 4. Computed and Experimental Bond Distances (Å) and Angles (deg) for (^{Et}PDI)$_2$Fe and (^{iPr}APDI)$_2$Fe

	(^{Et}PDI)$_2$Fe		(^{iPr}APDI)$_2$Fe	
	experimental	calculated	experimental	calculated
Fe(1)−N(1)	2.1246(16)	2.157	2.252(2)	2.232
Fe(1)−N(2)	1.9853(15)	1.984	2.0180(17)	2.041
Fe(1)−N(3)	2.5579(16)	2.517	2.2506(19)	2.275
Fe(1)−N(4)	2.1098(16)	2.124	2.259(2)	2.266
Fe(1)−N(5)	1.9864(15)	1.991	2.0236(18)	2.042
Fe(1)−N(6)	2.6096(16)	2.589	2.1846(18)	2.234
N(1)−C(2)	1.332(2)	1.340	1.316(3)	1.326
N(2)−C(3)	1.390(2)	1.386	1.399(3)	1.383
N(2)−C(7)	1.367(2)	1.381	1.362(3)	1.382
N(3)−C(8)	1.291(2)	1.317	1.299(3)	1.324
C(2)−C(3)	1.435(2)	1.453	1.431(3)	1.462
C(7)−C(8)	1.478(2)	1.467	1.457(4)	1.464
N(4)−C(31)/C(17)	1.334(3)	1.341	1.312(3)	1.325
N(5)−C(36)/C(22)	1.369(2)	1.379	1.387(3)	1.382
N(5)−C(32)/C(18)	1.387(2)	1.387	1.358(3)	1.383
N(6)−C(37)/C(23)	1.291(2)	1.314	1.304(3)	1.325
C(36)/C(22)−C(37)/C(23)	1.481(3)	1.469	1.426(3)	1.463
C(31)/C(17)−C(32)/C(18)	1.435(3)	1.453	1.450(4)	1.463
N(1)−Fe(1)−N(3)	78.99(6)	78.9	149.37(7)	150.01
N(4)−Fe(1)−N(6)	79.44(6)	79.8	149.06(7)	150.04
N(1)−Fe(1)−N(4)	101.15(6)	97.5	94.99(7)	93.39
N(2)−Fe(1)−N(5)	138.95(6)	145.6	176.90(8)	177.42

Computational Studies. Broken symmetry (BS) density functional theory (DFT) calculations were performed to further elucidate the electronic structure of the neutral bis(chelate)iron compounds. Two representative examples, four-coordinate (^{Et}PDI)$_2$Fe and six-coordinate (^{iPr}APDI)$_2$Fe, were examined as these compounds were crystallographically characterized and studied by Mössbauer spectroscopy. Ground-state geometries were optimized using experimentally determined $S = 1$ spin states applying the BP86 functional. The experimental and calculated geometric structures are in excellent agreement. Selected bond distances and angles are reported in Table 4. Single-point calculations on the optimized structures were performed at the B3LYP level of DFT. For both $S = 1$ complexes, the robustness of the BS solutions was checked by complementary calculations without broken symmetry. In both cases, the latter calculations resulted in a significantly (>10 kcal mol^{-1}) higher energy state.

The obtained broken symmetry (4,2) minimum is consistent with a high-spin ferrous ($S_{Fe} = 2$) center antiferromagnetically coupled to two ligand centered radicals—one on each chelate. Qualitative molecular orbital diagrams for both compounds are presented in Figure 8. For both compounds, five principally iron-based d orbitals were identified. One cloverleaf d orbital was found in both the spin-up and spin-down manifolds and is therefore doubly occupied. The other four were located in the spin-up manifold only and are singly occupied. Additionally, two ligand-centered orbitals with

(23) Carver, G.; Dobe, C.; Jensen, T. B.; Tregenna-Piggott, P. L. W.; Janssen, S.; Bill, E.; McIntyre, G. J.; Barra, A.-L. *Inorg. Chem.* **2006**, *45*, 4695.
(24) Reif, W. M., Jr.; Erickson, N. E. *J. Am. Chem. Soc.* **1968**, *90*, 4794.

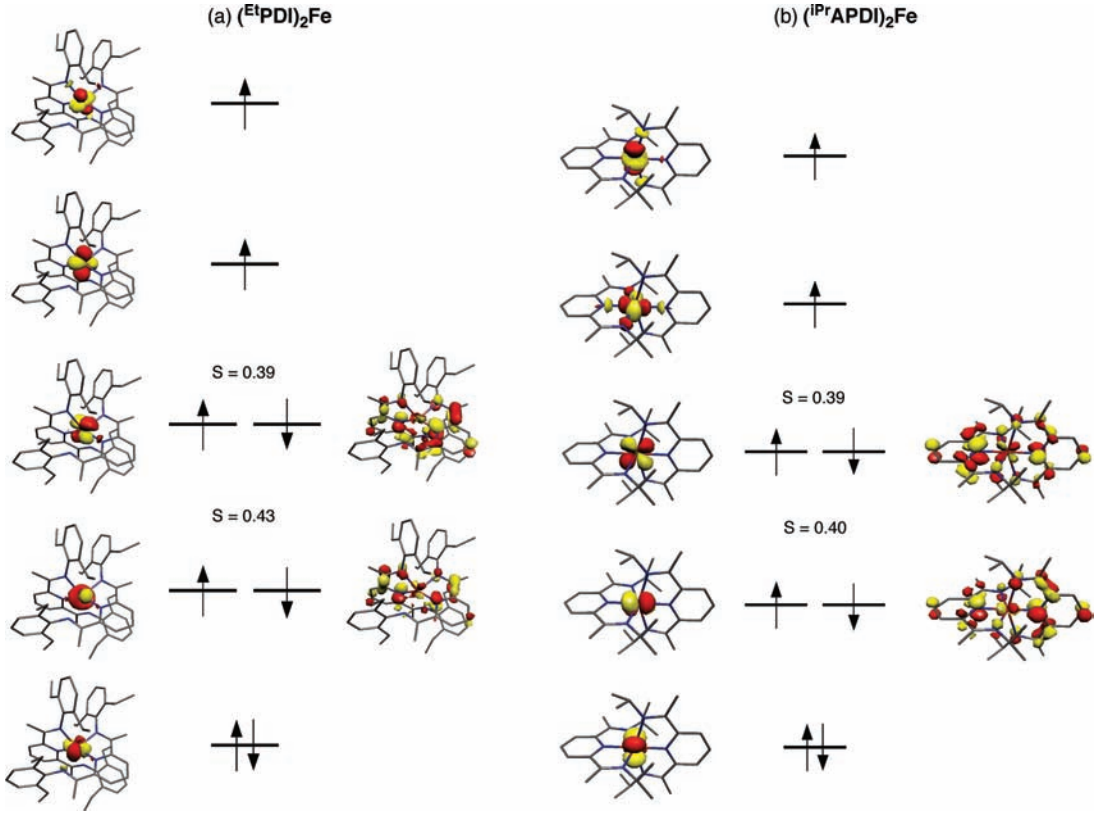

Figure 8. Qualitative molecular orbital diagram of the magnetic orbitals derived from BS(4,2) calculations of (a) $(^{Et}PDI)_2Fe$ and (b) $(^{iPr}APDI)_2Fe$. The spatial overlap (S) of corresponding α and β orbitals is given. Orbital energies are not to scale.

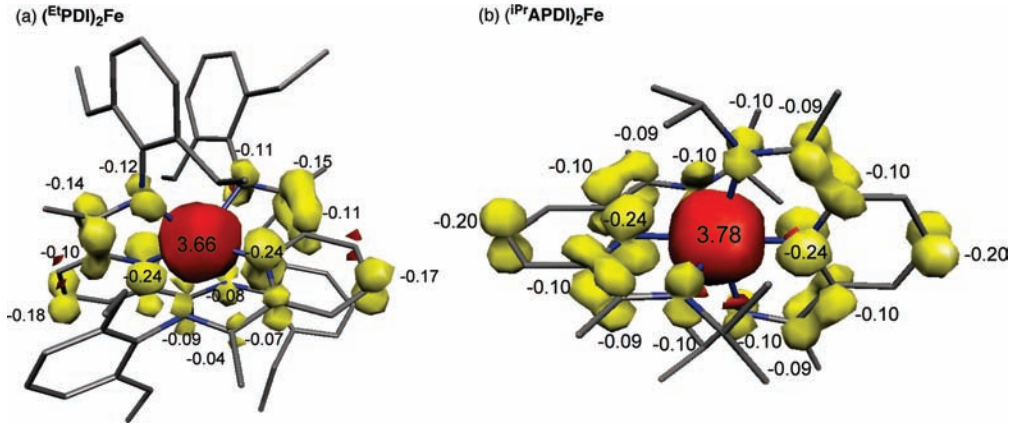

Figure 9. Spin density plots for (a) $(^{Et}PDI)_2Fe$ and (b) $(^{iPr}APDI)_2Fe$ derived from the BS(4,2) calculation (based on a Mulliken spin population).

minimal metal character were identified in the spin-down manifold and correspond to two symmetry-adapted linear combinations of the semioccupied molecular orbitals (SOMOs) of the two ligand radicals. Antiferromagnetic coupling of these two electrons with iron d orbitals of appropriate symmetry and energy accounts for the overall $S = 1$ magnetic state. The value of "S" denoted in both molecular orbital diagrams is the spatial overlap of the two SOMOs. A value of $S = 1$ indicates a standard, doubly populated molecular orbital with little spin polarization, while values of $S \ll 1$ indicate nonorthogonal magnetic orbital pairs.[25]

For pseudo-octahedral $(^{iPr}APDI)_2Fe$, the frontier molecular orbital representations shown in Figure 8 comprise a classic d-orbital splitting diagram, as expected from ligand field theory. Three cloverleaf d orbitals, nominally d_{xz}, d_{yz}, and d_{xy}, comprise a low energy "t_{2g}" set, while $d_{x^2-y^2}$ and d_{z^2} define an "e_g" set and are found higher in energy. Using the coordinate axis defined by the highest-energy d orbital (e.g. d_{z^2}), antiferromagnetic coupling occurs with bis(imino)pyridine SOMOs and d_{xy} and d_{yz}. Notably, the population of essentially σ^* molecular orbitals accounts for the observed elongation of the iron−nitrogen bonds in the neutral bis(chelate)iron compounds in the solid state, relative to their low-spin dicationic counterparts.

The computed spin density plots for both compounds (Figure 9) highlight the antiparallel spin alignment between the high-spin ferrous center and the π radical chelates.

(25) Neese, F. *J. Phys. Chem. Solids* **2004**, *65*, 781.

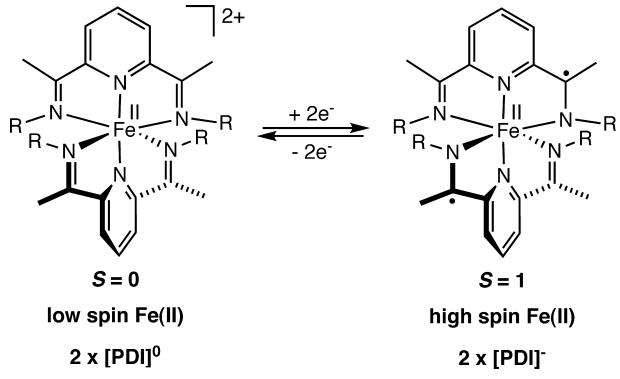

Figure 10. Change in spin state upon reduction of $[(PDI)_2Fe]^{2+}$ compounds.

Analysis of the spin density in terms of individual atomic contributions supports four unpaired electrons on the iron (3.66 for $(^{Et}PDI)_2Fe$ and 3.78 for $(^{iPr}APDI)_2Fe$) and one electron on each ligand. For the ligand-centered π radicals, the spin density is concentrated on the imine arms, pyridine nitrogen, and *ortho*- and *para*-pyridine carbons. Due to the lower symmetry in four-coordinate $(^{Et}PDI)_2Fe$, the spin density distribution on the ligand is asymmetric. The majority of the spin density is localized on the pyridine and the coordinated imine "arm" of the ligand, in agreement with the differences in the observed bond lengths for the two "arms".

Mössbauer parameters were also computed for $(^{Et}PDI)_2Fe$ and $(^{iPr}APDI)_2Fe$ to calibrate the computational results.[26,27] As reported in Table 5, the calculations on both compounds successfully reproduce the experimentally observed isomer shifts and are fully consistent with high-spin iron(II). Unfortunately, the experimental quadrupole splittings were not successfully reproduced by the calculations.[28]

The combined magnetic, structural, Mössbauer, and computational data obtained for both $(^{Et}PDI)_2Fe$ and $(^{iPr}APDI)_2Fe$ firmly establish the electronic structure of the compounds as containing a high-spin ferrous ion antiferromagnetically coupled to two bis(imino)pyridine radical anions. Thus, the (electro)chemical reduction of $[(PDI)_2Fe]^{2+}$ compounds to neutral $[(PDI)_2Fe]^0$ derivatives is ligand-based; the ferrous oxidation state is preserved throughout the reaction. However, the reduction of the bis(imino)pyridine from its neutral to monoanionic form decreases its π-acceptor ability and hence its ligand field strength, inducing a spin change from low to high spin at the iron center (Figure 10).

The effect of the ligand reduction in iron chemistry, namely, changing the spin state from low-spin iron(II) to high-spin, is opposite that of previous reports for related bis(chelate)manganese compounds.[11] For Mn, two-electron reduction of the high-spin ($S = 5/2$) $[(^{4\text{-}OMe}PDI)_2Mn^{II}]^{2+}$ complex yields the diamagnetic $[(^{MeO}PDI^-)_2Mn^{III}]^+$ compound. Thus, one-electron reduction of each chelate induces a spin change from high-spin Mn(II) to low-spin Mn(III). The origin of the apparently divergent effects in Fe and Mn chemistry is likely a result of the electronic configuration of the metal and its ability to engage in different π interactions with each oxidation state of the bis(imino)pyridine. The d^6 configuration of low-spin iron(II) is well-suited for π-backbonding with the empty π^* orbitals of a neutral bis(imino)pyridine. Reduction of the ligand to the monoanionic form, $[PDI]^-$, reduces its π-acidity and hence increases its π-basicity. High-spin Fe(II) is a relatively weak π donor (compared to low-spin Fe(II)) and a stronger π acceptor and is well matched with $[PDI]^-$.

Table 5. Experimental and Computed (in Parentheses) Zero-Field Mössbauer Parameters for $(^{Et}PDI)_2Fe$ and $(^{iPr}APDI)_2Fe$

	$(^{Et}PDI)_2Fe$	$(^{iPr}APDI)_2Fe$
δ (mm s^{-1})	0.91, 0.92 (0.72)	0.93 (0.82)
ΔE_Q (mm s^{-1})	1.52, 1.95 (4.10)	0.24 (1.22)

In manganese chemistry, reduction of the bis(imino)pyridine in the bis(chelate) compound again converts the ligand from its neutral π-accepting $[PDI]^0$ form to a more π-donating $[PDI]^-$ configuration. Low-spin Mn(III) favors interaction with a π-donating ligand and hence exhibits the opposite effect of the iron chemistry; namely, a spin state change from high-spin Mn(II) to low-spin Mn(III) accompanies ligand reduction. Thus, the appropriate match of ligand and metal oxidation state determines the influence of ligand reduction on the spin state of the resulting metal ion.

Concluding Remarks. Attempts to prepare analogs of the iron precatalyst, $(^{iPr}PDI)Fe(N_2)_2$, by sodium amalgam reduction of the corresponding iron dihalide bearing smaller aryl or alkyl imine substituents resulted in isolation of the neutral bis(chelate)iron compounds. These species, previously generated electrochemically, were described as too reducing to isolate. Characterization of the compound with 2,6-diethyl phenyl substituents by X-ray crystallography established a distorted tetrahedral compound with two κ^2-bis(imino)pyridines. Compounds with 4-OCH_3-substituted phenyl or alkyl imine substituents were also structurally characterized and found to have hexacoordinate geometries. For both the four- and six-coordinate compounds, the metrical parameters, Mössbauer isomer shifts, magnetic data, and open-shell, broken-symmetry DFT calculations support high-spin ferrous ions antiferromagnetically coupled to two chelate radical anions. Thus, the previously reported electrochemical reduction of diamagnetic $[(PDI)_2Fe]^{2+}$ to $[(PDI)_2Fe]$ occurs at the ligand, while the ferrous oxidation state is preserved. Notably, the neutral $[(PDI)_2Fe]$ compounds undergo a spin change from low- to high-spin iron(II), a result of a weaker-field, less-π-acidic bis(imino)pyridine chelate upon single-electron reduction.

Experimental Section

General Considerations. All air- and moisture-sensitive manipulations were carried out using standard vacuum line, Schlenk, and cannula techniques or in an MBraun inert atmosphere dry box containing an atmosphere of purified nitrogen. Solvents for air- and

(26) Neese, F. *Inorg. Chim. Acta* **2002**, *337*, 181.
(27) Sinnecker, S.; Slep, L. D.; Bill, E.; Neese, F. *Inorg. Chem.* **2005**, *44*, 2245.
(28) Calculations on $(^{iPr}APDI)_2Fe$ were also run with the COSMO package. Geometry optimization yielded $\delta = 0.83$ mm/s and $\Delta E = 1.222$ mm/s. Repeating the calculation with fixed coordinates from the experimentally determined X-ray structure, $\delta = 0.78$ mm/s and $\Delta E = 1.072$ mm/s. While the calculations do not successfully reproduce the quadrupole splittings, we believe this has little impact on conclusions about the electronic structure of the bis(chelate) complexes.

Table 6. Crystallographic Parameters for (^{Et}PDI)$_2$Fe, ($^{4\text{-OMe}}$PDI)$_2$Fe, (^{Cy}APDI)$_2$Fe, and (^{iPr}APDI)$_2$Fe

	(^{Et}PDI)$_2$Fe	($^{4\text{-OMe}}$PDI)$_2$Fe	(^{Cy}APDI)$_2$Fe	(^{iPr}APDI)$_2$Fe
empirical formula	$C_{126}H_{164}N_{12}Fe_2O_2$	$C_{46}H_{46}FeN_6O_4$	$C_{42}H_{62}N_6Fe$	$C_{30}H_{46}N_6Fe$
fw	1990.39	802.74	706.83	546.58
cryst dimensions	0.30 × 0.20 × 0.10	0.30 × 0.25 × 0.20	0.40 × 0.25 × 0.10	0.40 × 0.15 × 0.10
cryst syst	triclinic	monoclinic	monoclinic	monoclinic
space group	$P\bar{1}$	$P2/c$	$P2(1)/n$	$P2(1)/c$
a (Å)	12.136(2)	18.0838(14)	16.3610(9)	9.7390(5)
b (Å)	19.040(3)	15.9439(19)	13.2578(8)	16.4698(8)
c (Å)	23.774(4)	15.4641(16)	18.1805(9)	20.7204(10)
α (deg)	92.268(9)	90	90	90
β (deg)	102.270(8)	91.886(4)	96.083(2)	119.165 (2)
γ (deg)	90.946 (8)	90	90	90
V (Å^3)	5362.3 (16)	4456.3(8)	3921.3 (4)	2902.2 (2)
Z	2	4	4	4
ρ_{calcd} (g cm^{-3})	1.233	1.196	1.197	1.251
μ (mm^{-1})	0.329	0.386	0.421	0.549
F(000)	2144	1688	1528	1176
μ range (deg)	1.72−28.28	1.70 to 24.71	1.77−20.82	1.67−26.37
	$-16 \le h \le 15$	$-21 \le h \le 21$	$-16 \le h \le 15$	$-11 \le h \le 12$
	$-25 \le k \le 25$	$-18 \le k \le 18$	$-13 \le k \le 12$	$-16 \le k \le 20$
	$-31 \le l \le 31$	$-18 \le l \le 18$	$-15 \le l \le 18$	$-25 \le l \le 25$
total data collected	137395	30244	17487	26087
ind reflns	26277	7585	4096	5867
R_{int}	0.0388	0.0710	0.0583	0.0651
abs correction	semiempirical by SADABS	semiempirical from equivalents	semiempirical from equivalents	semiempirical from equivalents
range of transmission	0.9678−0.9076	0.9269−0.8931	0.9591−0.8496	0.9472−0.8104
refinement method	full-matrix least squares on F^2	full-matrix least squares on F^2	full-matrix least squares on F^2	full-matrix least squares on F^2
data/restraints/params	26277/0/1530	7585/0/515	4096/1146/611	5867/1/372
R_1 [$F_o^2 \ge 2\sigma(F_o^2)$]	0.0472	0.0500	0.0598	0.0491
wR_2 [$F_o^2 \ge -3\sigma(F_o^2)$]	0.1356	0.1187	0.1173	0.1074
goodness-of-fit	1.038	0.972	1.071	1.012
largest peak, hole (eÅ^{-3})	1.171, −0.824	0.313, −0.509	0.214, −0.247	0.366, −0.355

moisture-sensitive manipulations were initially dried and deoxygenated using literature procedures.[29] Hydrogen and deuterium gas were passed through a column containing manganese oxide supported on vermiculite and 4 Å molecular sieves before admission to the high-vacuum line. Benzene-d_6 and toluene-d_8 were purchased from Cambridge Isotope Laboratories and dried over 4 Å molecular sieves and titanocene, respectively. The iron dihalide compounds, (^{Et}PDI)FeBr$_2$,[30] ($^{4\text{-OMe}}$PDI)FeBr$_2$,[20] (^{Cy}APDI)FeBr$_2$,[31] (^{iPr}APDI)FeBr$_2$,[31] and (^{Myr}APDI)FeBr$_2$,[32] were prepared according to literature procedures.

^{1}H NMR spectra were recorded on Varian Mercury 300 and Inova 400 and 500 spectrometers operating at 299.76, 399.78, and 500.62 MHz, respectively. ^{2}H NMR spectra were recorded at 20 °C on the Inova 400 and 500 spectrometers operating at 61.37 and 76.85 MHz, respectively. All ^{1}H NMR chemical shifts are reported relative to SiMe$_4$ using residual chemical shifts of the solvent as a secondary standard. Solution magnetic moments were determined by the Evans method[33] using a ferrocene standard and are the average value of at least two independent measurements. ^{1}H NMR multiplicity and coupling constants are reported where applicable. Peak width at half-height is given for paramagnetically broadened resonances. Elemental analyses were performed at Robertson Microlit Laboratories, Inc., in Madison, New Jersey. All electronic absorption data were collected in toluene solution on a Shimadzu UV-2101 PC scanning spectrophotometer. Solid-state magnetic susceptibilities were determined at 23 °C using a Johnson Mathey magnetic susceptibility balance calibrated with HgCo(SCN)$_4$.

SQUID magnetization data of crystalline powdered samples were recorded with a SQUID magnetometer (Quantum Design) at 1 T between 5 and 300 K and at 1, 3, and 5 T in the range 2−30 K. Samples used for magnetization measurements were recrystallized multiple times and checked for chemical composition and purity by elemental analysis (C, H, and N) and ^{1}H NMR spectroscopy. Reproducibility was checked by collecting data on three independently synthesized samples. The experimental data were corrected for underlying diamagnetism by use of tabulated Pascal's constants[34,35] as well as for temperature-independent paramagnetism. The susceptibility and magnetization data were simulated with our simulation julX for exchange-coupled systems.[36]

Single crystals suitable for X-ray diffraction were coated with polyisobutylene oil in a drybox, transferred to a nylon loop, and then quickly transferred to the goniometer head of a Bruker X8 APEX2 diffractometer equipped with a molybdenum X-ray tube (λ = 0.71073 Å). Preliminary data revealed the crystal system. A hemisphere routine was used for data collection and determination of the lattice constants. The space group was identified, and the data were processed using the Bruker SAINT+ program and corrected for absorption using SADABS. The structures were solved using direct methods (SHELXS), completed by subsequent Fourier synthesis, and refined by full-matrix least-squares procedures.

Mössbauer data were collected at 80 K on an alternating constant-acceleration spectrometer. The minimum experimental line width was 0.24 mm s^{-1} (full width at half-height). A constant sample temperature was maintained with an Oxford Instruments Variox or an Oxford Instruments Mössbauer-Spectromag 2000 cryostat. Reported isomer shifts (δ) are referenced to iron metal at 293 K.

(29) Pangborn, A. B.; Giardello, M. A.; Grubbs, R. H.; Rosen, R. K.; Timmers, F. J. *Organometallics* **1996**, *15*, 1518.
(30) Schmidt, R.; Welsh, M. B.; Palackal, S. J.; Alt, H. G. *J. Mol. Catal. A* **2002**, *179*, 155.
(31) Castro, P. M.; Lappalainen, K.; Ahlgrén, M.; Leskelä, M.; Repo, T. *J. Polym. Sci., Part A: Polym. Chem.* **2003**, *41*, 1380.
(32) Abu-Surrah, A. S.; Lappalainen, K.; Piironen, U.; Lehmus, P.; Repo, T.; Leskelä, M. *J. Organomet. Chem.* **2002**, *648*, 55.
(33) Sur, S. K. *J. Magn. Reson.* **1989**, *82*, 169.
(34) O'Connor, C. J. *Prog. Inorg. Chem.* **1982**, *29*, 203.
(35) Weast, R. C.; Astle, M. J. *CRC Handbook of Chemistry and Physics*; CRC Press Inc.: Boca Raton, FL, 1979.
(36) Bill, E. julX, available from http://ewww.mpi-muelheim.mpg.de/bac/logins/bill/julX_en.php (accessed Nov. 2008).

Quantum-Chemical Calculations. All DFT calculations were performed with the ORCA program package.[37] The geometry optimizations of the complexes were carried out at the BP86[38−40] level of DFT. Single-point calculations on the optimized geometries were carried out using the B3LYP[38,41,42] functional. This hybrid functional often gives better results for transition metal compounds than pure gradient-corrected functionals, especially with regard to metal−ligand covalency.[43] The all-electron Gaussian basis sets were those developed by the Ahlrichs group.[44,45] Triple-ζ-quality basis sets TZV(P) with one set of polarization functions on the metals and the atoms directly coordinated to the metal center were used.[45] For the carbon and hydrogen atoms, slightly smaller polarized split-valence SV(P) basis sets were used, which were of double-ζ quality in the valence region and contained a polarizing set of d functions on the non-hydrogen atoms.[44] Auxiliary basis sets used to expand the electron density in the resolution-of-the-identity approach were chosen[46−48] where applicable, to match the orbital basis.

The self-consistent field calculations were tightly converged (1×10^{-8} E_h in energy, 1×10^{-7} E_h in the density change, and 1×10^{-7} in maximum element of the DIIS error vector). The geometry optimizations for all complexes were carried out in redundant internal coordinates without imposing symmetry constraints. In all cases, the geometries were considered converged after the energy change was less than 5×10^{-6} E_h, the gradient norm and maximum gradient element were smaller than 1×10^{-4} E_h Bohr^{-1} and 3×10^{-4} E_h Bohr^{-1}, respectively, and the root-mean square and maximum displacements of all atoms were smaller than 2×10^{-3} b and 4×10^{-3} b, respectively.

Throughout this paper, we describe our computational results by using the BS approach by Ginsberg[49] and Noodleman et al.[50] Because several broken-symmetry solutions to the spin-unrestricted Kohn−Sham equations may be obtained, the general notation BS(m,n)[51] has been adopted, where m (n) denotes the number of spin-up (spin-down) electrons at the two interacting fragments. Canonical and corresponding orbitals,[25] as well as spin density plots, were generated with the program Molekel.[52]

Nonrelativistic single-point calculations on the optimized geometry were carried out to predict Mössbauer spectral parameters (isomer shifts and quadrupole splittings). These calculations employed the CP(PPP) basis set[26] for iron. The Mössbauer isomer shifts were calculated from the computed electron densities at the iron centers as previously described.[53]

Preparation of (^{Et}PDI)$_2$Fe. A 250 mL round-bottomed flask was charged with mercury (100.0 g, 498.5 mmol) and approximately 100 mL of pentane. Sodium metal (0.502 g, 21.8 mmol) was added slowly in small pieces to the flask with stirring, and the resulting amalgam was stirred for 20 min. A slurry of (^{Et}PDI)FeBr$_2$ (2.00 g, 3.12 mmol) in pentane (10 mL) was added, and the resulting reaction mixture was stirred for 24 h at ambient temperature. The solution was filtered through Celite, and pentane and other volatiles were removed in vacuo. The resulting brown solid was recrystallized from pentane and yielded 0.717 g (44%) of a dark brown solid identified as (^{Et}PDI)$_2$Fe. The addition of 1 equiv of ^{Et}PDI increased the yield to 55%. Anal. calcd for $C_{58}H_{70}N_6Fe$: C, 76.80; H, 7.78; N, 9.27. Found: C, 76.49; H, 7.65; N, 8.73. ^{1}H NMR (benzene-d_6, 293 K): δ 166.3 (7602 Hz), 58.7 (5291 Hz), 1.42 (359 Hz), −0.49 (186 Hz). Magnetic susceptibility: $\mu_{eff} = 2.7\mu_B$ (benzene-d_6, 293 K).

Preparation of ($^{4\text{-OMe}}$PDI)$_2$Fe. A 100 mL round-bottomed flask was charged with mercury (24.8 g, 124 mmol) and approximately 40 mL of toluene. Sodium metal (0.122 g, 5.31 mmol) was added slowly, in small pieces, to the mercury with stirring, and the resulting amalgam was stirred for 20 min to completely dissolve the metal. A slurry of ($^{4\text{-OMe}}$PDI)FeBr$_2$ (0.610 g, 1.04 mmol) in toluene (10 mL) was added, and the capped solution was stirred for 24 h at room temperature. The solution was filtered through Celite, and toluene and other volatiles were removed in vacuo. The resulting brown solid was rinsed twice with pentane and recrystallized from toluene to yield olive-green/brown crystals identified as ($^{4\text{-OMe}}$PDI)$_2$Fe (0.072 g, 0.090 mmol, 18% based on ($^{4\text{-OMe}}$PDI)FeBr$_2$). Anal. calcd for $C_{46}H_{46}N_6FeO_4$: C, 68.83; H, 5.78; N, 10.47. Found: C, 68.70; H, 5.79; N, 10.29. ^{1}H NMR (benzene-d_6, 293 K): δ 161.3 (3235 Hz), 113.9 (2302 Hz), 5.58 (112 Hz), 3.45 (20 Hz), 1.62 (18 Hz), 1.28 (21 Hz), −201.1 (4236 Hz). Magnetic susceptibility: $\mu_{eff} = 2.4\mu_B$ (benzene-d_6, 293 K).

Preparation of (^{Cy}APDI)$_2$Fe. This molecule was prepared in a similar manner to (^{Et}PDI)$_2$Fe with 0.438 g (0.81 mmol) of (^{Cy}APDI)FeBr$_2$ and 0.098 g (4.26 mmol) of sodium metal in 19.60 g (97.8 mmol) of mercury and 40 mL of toluene. Recrystallization from pentane at −35 °C yielded 0.189 g (66%) of a dark green solid identified as (^{Cy}APDI)$_2$Fe. Anal. calcd for $C_{42}H_{62}N_6Fe$: C, 71.37; H, 8.84; N, 11.89. Found: C, 71.08; H, 8.74; N, 11.49. ^{1}H NMR (benzene-d_6, 293 K): δ 227.5 (1407 Hz), 92.19 (747 Hz), 79.50 (943 Hz), 1.36 (m, 86 Hz), 0.58 (81 Hz), −3.24 (78 Hz), −154.9 (1477 Hz). Magnetic susceptibility: $\mu_{eff} = 2.5\mu_B$ (benzene-d_6, 293 K).

Preparation of (^{iPr}APDI)$_2$Fe. This molecule was prepared in a similar manner to (^{Et}PDI)$_2$Fe with 0.636 g (1.38 mmol) of (^{iPr}APDI)FeBr$_2$ and 0.159 g (6.92 mmol) of sodium metal in 31.80 g (159 mmol) of mercury and 100 mL of toluene. Recrystallization from pentane at −35 °C yielded 0.276 g (73%) of a dark green crystalline solid identified as (^{iPr}APDI)$_2$Fe. Anal. calcd for $C_{30}H_{46}N_6Fe$: C, 65.92; H, 8.48; N, 15.38. Found: C, 57.26; H, 7.36; N, 11.89. ^{1}H NMR (benzene-d_6, 293 K): δ 225.4 (1040 Hz), 87.57 (392 Hz), 81.25 (368 Hz), −18.17 (177 Hz), −158.4 (1394 Hz). Magnetic susceptibility: $\mu_{eff} = 3.3\mu_B$ (Gouy balance, 293 K).

Preparation of (^{Myr}APDI)$_2$Fe. This molecule was prepared in a similar manner to (^{Et}PDI)$_2$Fe with 0.268 g (0.42 mmol) of (^{Myr}PDI)FeBr$_2$ and 0.053 g (2.30 mmol) of sodium metal in 9.54 g (47.6 mmol) of mercury and 40 mL of toluene. Recrystallization from pentane at −35 °C yielded 0.120 g (63%) of a dark green

(37) Neese, F. *Orca*, version 2.6, revision 4; Institut für Physikalische und Theoretische Chemie, Universität Bonn: Bonn, Germany, 2007.
(38) Becke, A. D. *J. Chem. Phys.* **1986**, *84*, 4524.
(39) Perdew, J. P.; Yue, W. *Phys. Rev. B: Condens. Matter Mater. Phys.* **1986**, *33*, 8800.
(40) Perdew, J. P. *Phys. Rev. B: Condens. Matter Mater. Phys.* **1986**, *33*, 8822.
(41) Becke, A. D. *J. Chem. Phys.* **1993**, *98*, 5648.
(42) Lee, C. T.; Yang, W. T.; Parr, R. G. *Phys. Rev. B: Condens. Matter Mater. Phys.* **1988**, *37*, 785.
(43) Neese, F; Solomon, E. I. In *Magnetoscience: From Molecules to Materials*; Miller, J. S., Drillon, M., Eds.; Wiley: New York, 2002; Vol. *4*, p 345.
(44) Schäfer, A.; Horn, H.; Ahlrichs, R. *J. Chem. Phys.* **1992**, *97*, 2571.
(45) Schäfer, A.; Huber, C.; Ahlrichs, R. *J. Chem. Phys.* **1994**, *100*, 5829.
(46) Eichkorn, K.; Weigend, F.; Treutler, O.; Ahlrichs, R. *Theor. Chem. Acc.* **1997**, *97*, 119.
(47) Eichkorn, K.; Treutler, O.; Öhm, H.; Häser, M.; Ahlrichs, R. *Chem. Phys. Lett.* **1995**, *240*, 283.
(48) Eichkorn, K.; Treutler, O.; Öhm, H.; Häser, M.; Ahlrichs, R. *Chem. Phys. Lett.* **1995**, *242*, 652.
(49) Ginsberg, A. P. *J. Am. Chem. Soc.* **1980**, *102*, 111.
(50) Noodleman, L.; Peng, C. Y.; Case, D. A.; Mouesca, J. M. *Coord. Chem. Rev.* **1995**, *144*, 199.
(51) Kirchner, B; Wennmohs, F.; Ye, S.; Neese, F. *Curr. Opin. Chem. Biol* **2007**, *11*, 134.
(52) Molekel, Advanced Interactive 3D-Graphics for Molecular Sciences, available under http://www.cscs.ch/molekel/ (accessed Nov. 2008).
(53) Sinnecker, S.; Slep, L. D.; Bill, E.; Neese, F. *Inorg. Chem.* **2005**, *44*, 2245.

crystalline solid identified as (^{Myr}APDI)$_2$Fe. Anal. calcd for $C_{58}H_{84}N_6Fe$: C, 75.62; H, 9.19; N, 9.12. Found: C, 75.53; H, 9.54; N, 8.71. ^{1}H NMR (benzene-d_6, 293 K): δ 189.8 (3115 Hz), 110.0 (2455 Hz), 72.3 (2823 Hz), 1.6 (52 Hz), 1.18 (m, 91 Hz), 0.75 (38 Hz), 0.10 (146 Hz), −55.4 (3777 Hz), −176.9 (5055 Hz). Magnetic susceptibility: $\mu_{eff} = 1.8\mu_B$ (benzene-d_6, 293 K).

Crystallographic parameters for (^{Et}PDI)$_2$Fe, ($^{4\text{-}OMe}$PDI)$_2$Fe, (^{Cy}APDI)$_2$Fe, and (^{iPr}APDI)$_2$Fe are given in Table 6.

Spectroscopic Data for Bis(imino)pyridine Iron Dihalide Compounds.

Characterization of (^{Et}PDI)FeBr$_2$. ^{1}H NMR (CD_2Cl_2): δ 77.39 (41 Hz, 2H, *m*-py), 61.07 (30 Hz, 1H, *p*-py), 15.90 (20 Hz, 4H, *m*-Ar), 9.69 (204 Hz, 4H, CH_2CH_3), 8.84 (151 Hz, 4H, CH_2CH_3), −2.60 (34 Hz, 12H, CH_2CH_3), −11.51 (20 Hz, 2H, *p*-Ar), −24.30 (34 Hz, 6H, N=CCH_3).

Characterization of ($^{4\text{-}OMe}$PDI)FeBr$_2$. ^{1}H NMR (DMSO-d_6, 293 K): δ 8.44 (d, $^3J_{HH} = 8.0$ Hz, 2H, *m*-py), 8.28 (t, $^3J_{HH} = 8.0$ Hz, 1H, *p*-py), 6.67 (d, $^3J_{HH} = 9.2$ Hz, 4H, Ar−H), 6.16 (d, $^3J_{HH} = 9.2$ Hz, 4H, Ar−H), 3.63 (s, 6H, OCH_3), 2.59 (s, 6H, N=CCH_3).

Characterization of (^{Cy}APDI)FeBr$_2$. ^{1}H NMR (CD_2Cl_2, 293 K): δ 175.05 (126 Hz, 2H, CyCH), 72.59 (23 Hz, 2H, *m*-py), 37.52 (17 Hz, 1H, *p*-py), 7.27 (229 Hz, 4H, $CyCH_2$), 2.44 (32 Hz, 4H, $CyCH_2$), 0.65 (24 Hz, 4H, $CyCH_2$), 0.33 (15 Hz, 4H, $CyCH_2$), −11.25 (57 Hz, 6H, $N = CCH_3$), −18.48 (100 Hz, 4H, $CyCH_2$).

Characterization of (^{iPr}APDI)FeBr$_2$. ^{1}H NMR (CD_2Cl_2, 293 K): δ 176.04 (458 Hz, 2H, ^{i}PrCH), 74.38 (194 Hz, 2H, *m*-py), 32.46 (521 Hz, 1H, *p*-py), 0.40 (840 Hz, 12H, ^{i}PrCH$_3$), −11.49 (148 Hz, 6H, N=CCH_3).

Characterization of (^{Myr}APDI)FeBr$_2$. ^{1}H NMR (DMSO-d_6, 293 K): δ 8.90 (d, $^3J_{HH} = 8.0$ Hz, 2H, *m*-py), 8.77 (t, $^3J_{HH} = 8.0$ Hz, *p*-py), 3.12 (t, $^3J_{HH} = 12.4$ Hz, 2H, CH), 2.72 (s, 6H, $N = CCH_3$), 2.06 (s, 2H, CH), 0.93 (s, 2H, CH), 0.81 (s, 6H, CH_3), 0.77−0.64 (m, 6H), 0.50 (s, 2H, CH), 0.39 (d, $^3J_{HH} = 9.2$ Hz, 2H, CH).

Supporting Information Available: Crystallographic data for (^{Et}PDI)$_2$Fe, ($^{4\text{-}OMe}$PDI)$_2$Fe, (^{Cy}APDI)$_2$Fe, and (^{iPr}APDI)$_2$Fe in CIF format. Representative electronic absorption spectra and a Curie plot. This material is available free of charge via the internet at http://pubs.acs.org.

Acknowledgment. We thank the Packard Foundation (Fellowship in Science and Engineering to P.J.C.) and the U.S. National Science Foundation and Deutsche Forschungsgemeinschaft for a Cooperative Activities in Chemistry between U.S. and German Investigators grant.

IC801623M